Effect of Finger Orientation on Contact Stiffness and Area During Sliding

Jahangier Ahmad†, Easa AliAbbasi†, MReza Alipour Sormoli, and Cagatay Basdogan*

***Abstract*—Earlier experimental studies showed that the apparent contact area of a human fingerpad shrinks and eventually reaches a steady-state value as it slides on a smooth surface, although the root causes of this reduction have not been fully understood yet. We hypothesize that finger rotation about its axial axis and the movement direction play critical roles in the area change. To test this hypothesis, we conducted an experimental study to investigate the evolution of apparent contact area between a human fingerpad and a smooth flat surface under normal loading (stationary finger) and combined loading (sliding finger) conditions for 4 different internal rotations of the index finger (away from the second finger) about its axial (longitudinal) axis and 2 different sliding directions. Our results show a reduction in the contact area for radial sliding as expected, but a surprising increase in the ulnar direction for the higher finger rotations. We argue that this asymmetric behavior in contact area evolution stems from the changes in the equivalent radius of curvature and stiffening of the finger as the rotation angle increases, which manifests itself as the asymmetric stress distribution at the leading and trailing edges of the fingerpad in our finite element simulations.**

***Index Terms*—contact mechanics, sliding friction, touch, skin mechanics, finger contact area, finite element modeling.**

I. Introduction

CONTACT mechanics between a human fingerpad and a smooth surface has captured the interest of researchers due to its applications in various domains such as tribology, haptics, and robotics [1]–[3]. Comprehending the mechanics of human finger contact presents a formidable challenge, necessitating the application of advanced mathematical models due to the intricate interplay between normal (F_n) and tangential (F_t) forces during sliding. This challenge is compounded by the finger's complex morphological structure, hyper-viscoelastic material properties, and physiological characteristics.

During stationary contact with a smooth surface under normal loading, the apparent contact area of the fingerpad (A_{app}) increases non-linearly with the applied normal force, which can be estimated by the Hertz contact model. Johnson, Kendall, and Roberts (JKR) [4] improved the Hertz contact model by considering the adhesive interactions due to van der Waals forces. They estimated a greater contact area compared to the Hertzian prediction for a given normal force and showed that there exists a finite contact area even at zero normal force due to adhesion. In comparison to JKR theory, Derjaguin, Muller, and Toporov (DMT) [5] considered multiple contact points and accounted for both elastic and non-elastic deformations due to adhesive forces. Tabor [6] conducted further research and demonstrated that the JKR and DMT theories are actually specific scenarios within a broader framework that incorporates adhesion forces both inside and outside the contact region and concluded that adhesion between solids depends not only on surface forces but also on surface roughness and degree of ductility of the solids themselves. To consider the surface roughness, Greenwood and Williamson [7] assumed that the asperities of a rough surface in contact with a smooth surface vary randomly with some probabilistic distribution and the Hertz contact model is applicable for each asperity to calculate the total contact area. Persson [8] extended this probabilistic approach by considering the surface roughness at multiple length scales in which the asperities are of different heights and radii of curvature. In this approach, the real area of contact (A_{real}) is predicted to be much smaller than the apparent contact area [9], contingent upon factors such as the normal force, moisture level, and the duration of contact. For example, hydration (increase in moisture level) increases the apparent finger contact area due to the softening of the finger, also known as plasticization [10], [11], and the ratio of real to apparent contact areas [12].

The earlier studies also showed that the material properties of the finger significantly influence the size of the contact area. The human skin comprises multiple layers with different material properties, resulting in non-linear and time-dependent responses to the normal loading [13]–[16]. Dzidek et al. [17] proposed an elastic contact model based on a geometrical simplification of the fingerpad in which its secant modulus was found linearly proportional to the normal force. The results of their experiments, performed under normal loading up to 2 N, showed higher values of apparent contact area for a stationary finger inclined at 30° relative to a glass plate compared to that of 45°. Whereas, Young's modulus and the secant modulus of the fingerpad were reported higher for the 45° inclination than those of 30°.

In contrast to normal loading, contact mechanics of human finger sliding on a smooth surface under combined loading of normal and tangential forces has been investigated less in the literature since it is a more complex problem. The mechanisms contributing to the sliding friction include adhesion, deformation of asperities, plastic deformation at the contact interface, fracture, interlocking, finger moisture, and the contamination particles between the surfaces [1], [18]–[24]. In particular, the experimental studies show that adhesion plays an important role in finger friction during contact with a smooth surface [2], [24]–[27]. The friction coefficient is higher for the contacts with a smooth surface at low normal forces but reduces as the normal force is increased [25]. Moreover, the friction coefficient is influenced by the sliding direction. When sliding on sandpaper at a velocity of 20 mm/sec, the human finger exhibited a higher coefficient of friction in the proximal direction compared to the distal direction [28]. The earlier studies also show that the apparent contact area of the fingerpad reduces during sliding with the increase in tangential forces until reaching a steady-state value [29]–[31]. Delhaye et al. [29] measured the contact area between sliding human finger and a flat glass surface for 3 normal forces (0.5, 1, and 2 N) and 3 sliding velocities (5, 10, and 20 mm/s) along 4 anatomical directions (distal, proximal, radial, and ulnar). They reported a reduction of approximately 30% in the apparent contact area for all directions.

J. Ahmad, E. AliAbbasi, M. Alipour Sormoli, and C. Basdogan are with the College of Engineering, Koc University, Istanbul 34450, Turkey (E-mail: jahmad19@ku.edu.tr; ealiabbasi20@ku.edu.tr; msormoli18@ku.edu.tr; cbasdogan@ku.edu.tr).

E. AliAbbasi is also with Sensorimotor Interaction Group, Max Planck Institute for Informatics, Saarland Informatics Campus, Saarbrücken 66123, Germany (E-mail: easa.aliabbasi@mpi-inf.mpg.de).

*Corresponding author: cbasdogan@ku.edu.tr

†These authors contributed equally to this work and shared the first authorship.

Manuscript received XX XX, 202X; revised XX XX, 202x.

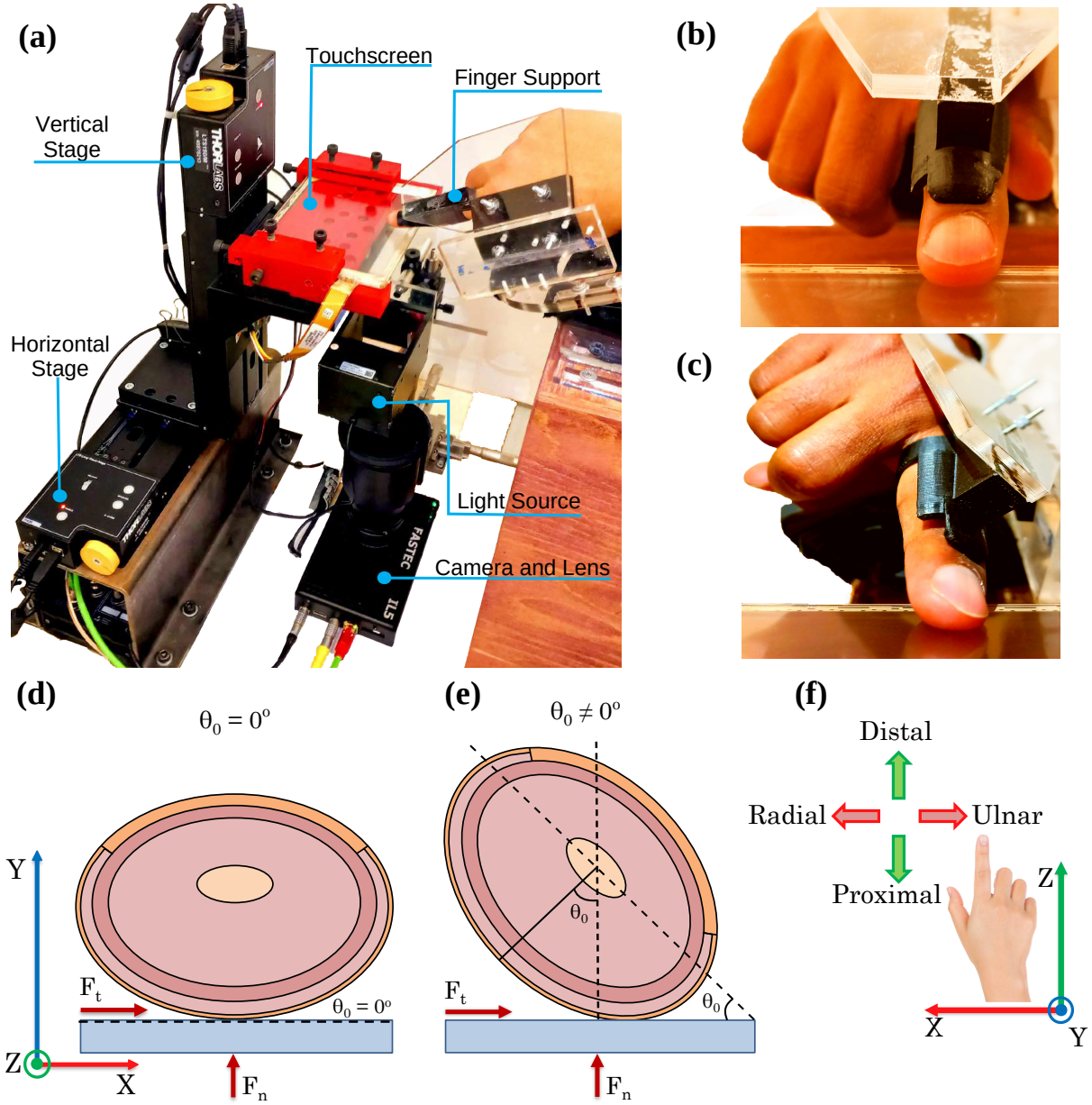

Fig. 1 (a) The experimental setup used in our study. The index finger of each participant was fixated using the finger support at internal rotation angles of $\theta_0 = 0°$, $15°$, $30°$, and $45°$ about the longitudinal axis of the finger. The normal force and sliding velocity were controlled by vertical and horizontal stages, respectively. The contact area was illuminated by a co-axial light source and imaged by a high-speed camera. Finger configurations for (b) $0°$ and (c) $45°$ internal rotation angles. The schematic cross-sectional views of the finger for the rotation angles of (d) $\theta_0 = 0°$ and (e) $\theta_0 \neq 0°$. (f) Coordinate axes and anatomical directions used in our study.

Similar results were also reported by Sahli et al. [30] for the contacts between a sliding human finger and a smooth surface. They showed that the reduction in contact area starts with the application of tangential forces and saturates well before macroscopic sliding. This suggests that assuming constant shear stress during sliding is reasonable for modeling adhesion-controlled friction [21]. Sahli et al. [22] also investigated anisotropic shearing of the contact area due to tangential force via a fracture mechanics model. They showed that in rough elastomer contacts, the shape of microjunctions changes significantly in response to the shear force applied to the interface. This results in increasing anisotropy of the overall contact interface, which eventually stabilizes in the macroscopic sliding regime.

Despite the experimental evidence, the contact mechanics behind the reduction in the apparent contact area of the sliding finger is still not fully understood. It has been argued that the non-linear material properties of the finger and stiffening in the direction of sliding play an important role [29]. Lengiewicz et al. [32] argued that the finite deformations govern the area reduction during sliding, with a dominating effect of local contact lifting at the trailing edge. Mergel et al. [23] developed a comprehensive computational framework for contact mechanics where adhesion and friction interact in a coupled manner. The model captures the dynamic interaction between these two forces, particularly in soft and elastic materials when in contact with smooth and flat surfaces. Their results indicate that shear-induced area reduction in these interfaces is not limited to (nearly) incompressible materials. Furthermore, they suggest that while adhesion is not essential for modeling this phenomenon, it amplifies the effect resulting from finite, non-linear material deformations.

We hypothesize that not only the non-linear stiffening and finite deformations of the finger but also the finger rotation about its axial axis affects the contact area during sliding on a smooth surface. Finger contacts with surfaces in our daily activities frequently involve rotation angles beyond zero degrees. Rotations higher than zero degrees are common when interacting with digital objects on the touchscreen of a cell phone, exploring the texture of a surface, or grasping and manipulating an object with multiple fingers. The earlier studies investigating the contact mechanics between the fingerpad and a smooth surface under normal or combined loading conditions mostly ignored the changes in contact area due to the rotation of the finger. However, the finger rotates slightly due to the tangential shear loading during sliding, and the contact area changes. Moreover, when grasping a curved object under normal loading or exploring an inclined surface under combined loading, our fingers can take different orientations relative to the contacted surface, and the contact area changes again. Under the contact conditions above, the equivalent radius of curvature, one of the factors affecting the apparent contact area, changes with the finger orientation since the cross-section of the human finger is elliptical and not circular. Moreover, the human finger exhibits a complex hierarchical structure, comprising multiple sub-structures, each characterized by distinct material properties. As the orientation of the finger changes, stiffening may occur, which may again affect the contact area.

To test our hypothesis, we conducted an experimental study to investigate the effect of finger rotation about its axial axis on the evolution of the apparent contact area of fingerpad i) under normal loading (stationary finger) and ii) under combined normal and tangential loading during sliding in ulnar and radial directions. The coefficient of sliding friction ($CoF = F_t/F_n$) was measured as a function of displacement under the sliding condition. To validate our experimental results and gain a deeper understanding of the contact mechanics between the human finger and a smooth surface, finite element modeling (FEM) simulations were performed in COMSOL Multiphysics for the conditions corresponding to our physical experiments. Our experimental and FEM results reveal a decrease in contact area for radial sliding, consistent with prior studies for the case of no rotation ($\theta_0 = 0^\circ$) [29], [30]. However, for the internal finger rotations of $\theta_0 = 30^\circ$ and 45°, an increase in the contact area was observed for ulnar sliding. To our knowledge, this is the first study in the literature reporting an increase in the apparent contact area for the sliding human finger. Additionally, we observed that steady-state CoF decreases with increased normal load, reflecting adhesion effects at low normal forces as reported in [2], [25]. The stiffening of the finger with an increase in rotation angle also contributes to decreased steady-state CoF due to a drop in apparent contact area.

II. Material and Methods

A. Subjects

Two male subjects participated in our experiments (S_1: 30 and S_2: 35 years old). Before the experiments, the subjects were instructed to read and sign a consent form that had been approved by Koc University's Ethical Committee for Human Participants. The experiment was carried out in compliance with pertinent rules and regulations and the study was conducted in accordance with the Declaration of Helsinki's tenets.

B. Experimental methods

We conducted experiments utilizing the setup devised in [33], [34], incorporating a customized 3D-printed finger-support mechanism for precise control over the internal rotation of the index finger about its longitudinal axis at four distinct angles ($\theta_0 = 0^\circ$, 15°, 30°, and 45°) relative to the surface of a touchscreen (SCT3250, 3M Inc.), as depicted in Fig. 1a. The finger was positioned at a 20° inclination relative to the touchscreen surface using custom-designed finger, arm, and hand supports. The touchscreen was mounted on two linear translational stages (LTS150, Thorlabs Inc.) to control its movements in normal and tangential directions relative to the index finger. In this study, the touchscreen was utilized as a smooth surface in which the fingerpad is in contact. Hence, it will be referred to as the "plate" in the remainder of this manuscript. A force transducer (Mini40-SI-80-4, ATI Industrial Automation Inc.) was placed beneath the plate to measure normal and tangential forces acting on the finger. A co-axial light source (C50C, Contrastech Inc.) and a high-speed camera (IL5H, Fastec Imaging Inc.) were used to capture the images of the fingerpad during the experiments. The normal and tangential forces acting on the finger were acquired by a DAQ card (PCIe-6034E, National Instruments) at a sampling frequency of 2.5 kHz. A proportional-integral-derivative (PID) controller was utilized to keep the normal force acting on the finger constant while sliding the plate underneath the finger in ulnar and radial directions with a desired velocity by moving the horizontal stage.

The prone position of the hand (palm facing down) relative to the plate, as shown in Fig. 1b, was referred to as 0° rotation. The finger rotations other than the prone position were attained by internal rotation of the right hand (for example, Fig. 1c illustrates 45° rotation). A custom-made finger support manufactured by a 3D printer was utilized to control the finger's rotation precisely at the desired angles. Schematic representations of the fingerpad's cross-section at rotation angles equal and not equal to zero degrees are presented in Fig. 1d and e, respectively. The 4 anatomical directions are illustrated in Fig. 1f.

Our experiments comprise two parts: i) stationary finger under normal loading and ii) sliding finger under combined normal and

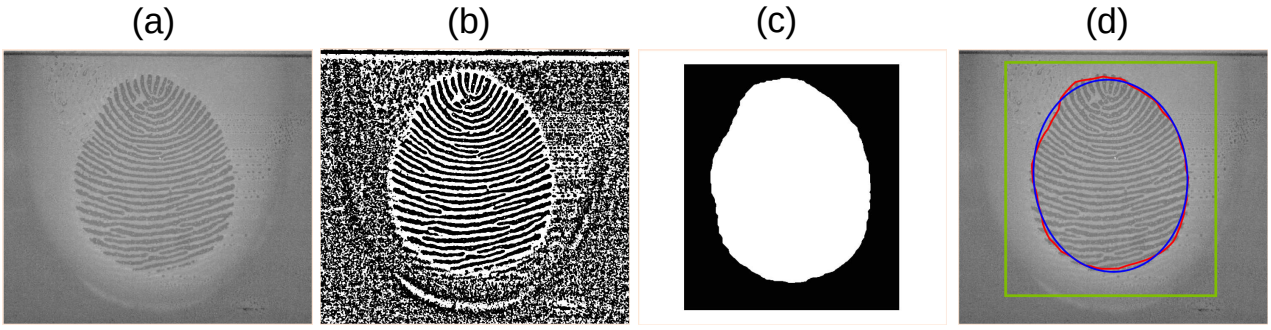

Fig. 2 Processing of fingerpad images: (a) raw image, (b) output of homomorphic filtering, (c) output of grayscale mathematical morphology. (d) The annotations made on the image (green: the selected rectangular sub-region, red: contour of the elliptical area, blue: fitted ellipse).

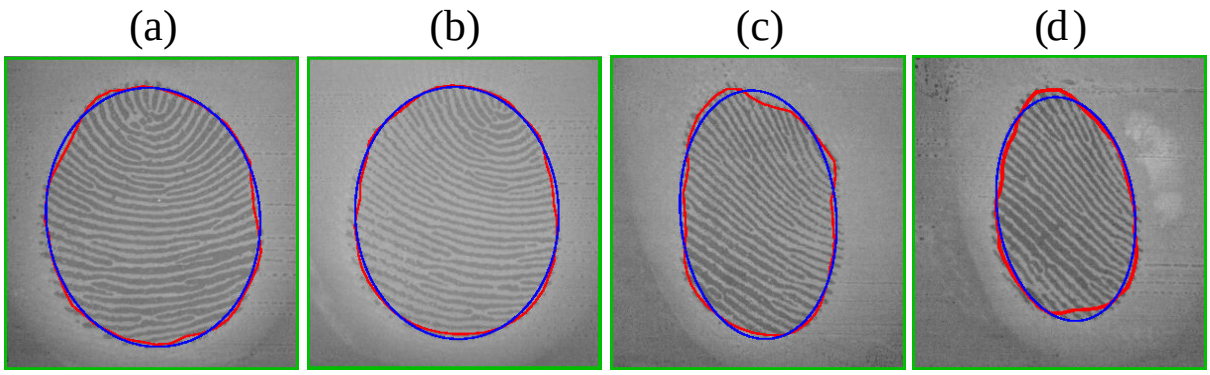

Fig. 3 Fingerpad images of S_1 under the normal force of 1 N for the initial rotation angles of (a) θ_0 = 0°, (b) θ_0 = 15°, (c) θ_0 = 30°, and (d) θ_0 = 45°.

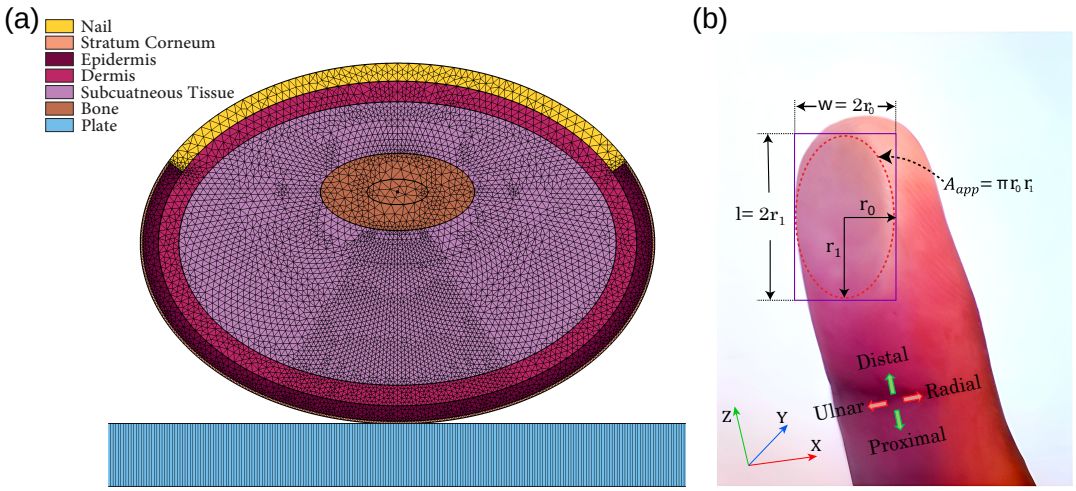

Fig. 4 (a) 2D FEM model of the finger in contact with the plate. In this model, subcutaneous tissue, dermis, and epidermis are defined as hyperelastic materials, and bone, nail, SC, and the plate are defined as stiff elastic materials. (b) The elliptical contact area of the fingerpad ($A_{app} = \pi r_0 r_1$) was calculated by using the width of contact, $w = 2r_0$, estimated by the FEM simulations and the contact length, $l = 2r_1$, measured by the experiments.

tangential loading. Before the experiments, the participants washed their hands with soap and water and dried them at room temperature. To ensure a good contrast in the captured fingerpad images, 0.5 μL of liquid vaseline was carefully applied to the participant's fingerpad using a micropipette. The participants were advised to remain stable throughout the experiments.

During the first experiment (stationary finger under normal loading), the plate was commanded to move 4.5 mm upwards in the normal direction with a step size of 0.1 mm. Between the steps, the plate stayed stationary for 10 seconds so that the normal force applied to the finger could reach a relaxation. We recorded the images of the apparent contact area and the normal forces during the last 2 seconds of the elapsed time. The apparent contact area was calculated using the approach suggested by [29], which involves homomorphic filtering of the raw images, identifying fingerpad contours by grayscale mathematical morphology, and fitting an ellipse to the contours as illustrated in Fig. 2. The area of the fitted ellipse was taken as the apparent contact area of the fingerpad. Fig. 3a, b, c, and d depict the fingerpad contact areas of S_1 for the initial rotation angles of 0°, 15°, 30°, and 45°, respectively.

In the second experiment (sliding finger under combined normal and tangential loading), we recorded the images of the fingerpad together with the normal and tangential forces acting on the finger while the plate was slid beneath the fingerpad with a constant velocity of 20 mm/s in ulnar and radial directions under 3 normal forces (0.5, 1, and 1.5 N). Each trial started by applying a desired normal force on the fingerpad and triggering the camera to record images, followed by the horizontal motion of the plate.

TABLE I Material properties of the fingerpad layers and plate used in the FEM model.

Layers	Hyperelastic (kPa)						Linear Elastic		
	C_{10}	C_{01}	C_{11}	C_{20}	C_{02}	(κ)	E (MPa)	ν	ρ (kg/m^3)
Subcutaneous Tissue	-59.6	64.0	-182.7	40.0	228.7	20.1	-	-	-
Dermis	-56.0	67.2	-182.7	42.5	228.7	49.4	-	-	-
Epidermis	-50.0	70.0	-182.7	48.5	228.7	92.3	-	-	-
Bone	-	-	-	-	-	-	17000	0.3	1908
Nail	-	-	-	-	-	-	17	0.3	1900
Stratum Corneum	-	-	-	-	-	-	1	0.3	1200
Plate	-	-	-	-	-	-	73100	0.3	2500

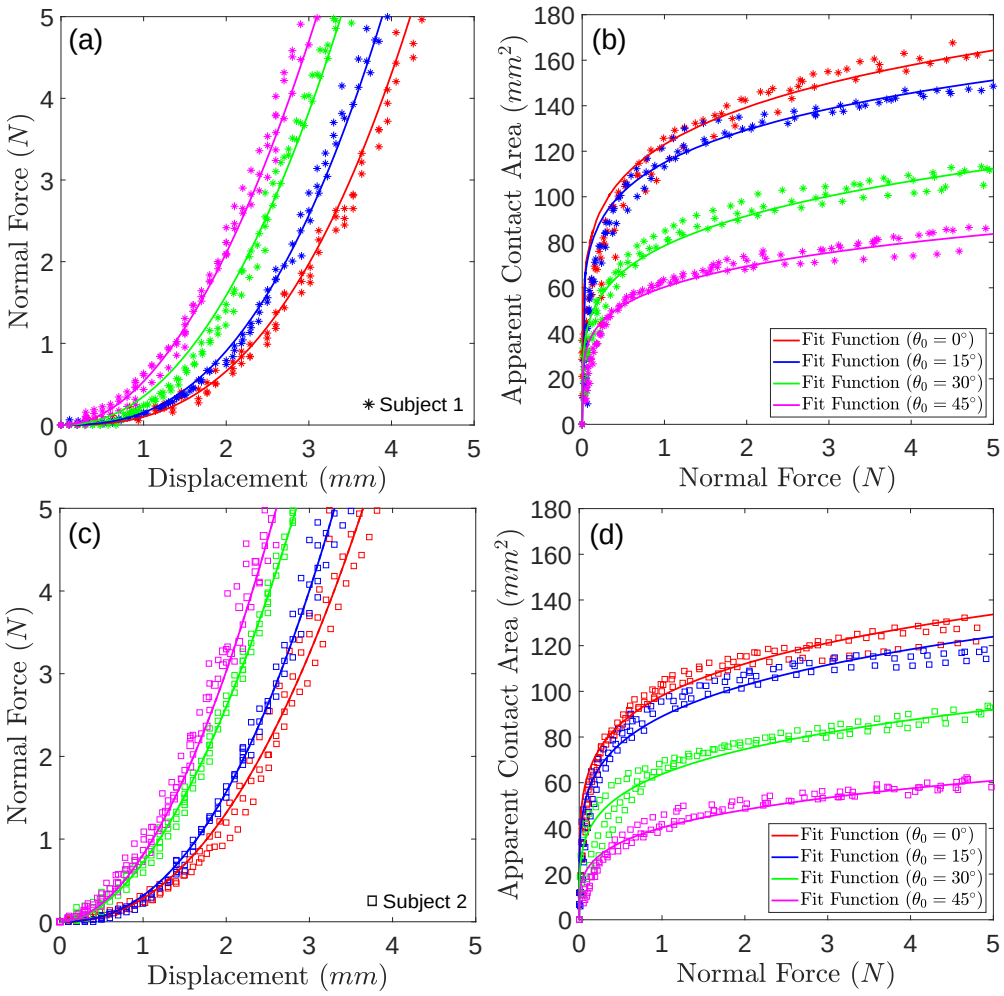

Fig. 5 Normal force acting on the fingerpad of subjects as a function of vertical displacement and the apparent contact area as a function of the normal force in normal loading condition (stationary finger) for 4 different rotations of the subjects' finger: the plots (a) and (b) are for subject S_1, and the plots (c) and (d) are for subject S_2.

C. Finite element modeling

A 2D elliptical FEM model of the human fingerpad in contact with a flat plate was developed in COMSOL Multiphysics to simulate contact interactions under pure normal loading (stationary finger) and combined loading conditions (sliding finger). The model of the finger contains the nail and 4 sub-layers, including Stratum Corneum (SC), epidermis, dermis, and subcutaneous tissue attached to the bone, as shown in Fig. 4a. The material properties of all layers are tabulated in Table I, which are adopted from literature [35]–[37]. The thickness of the SC, epidermis, and dermis layers are 0.1 mm, 0.6 mm, and 0.8 mm, respectively, and the major and minor radii of the 2D elliptical finger model are 10 mm and 7 mm, respectively. Five-parameter Mooney-Rivlin's material model was utilized for the dermis, epidermis, and subcutaneous tissue due to their hyperelastic behavior [38]. The FEM mesh comprised 21601 triangular elements (finger), 800 quadrilaterals (the plate), 5541 edge elements, and 368 vertex elements. To enforce the contact constraints, the "Penalty" contact method was utilized. The average static and dynamic coefficients of friction (CoFs), obtained from the experiments performed in this study, were incorporated into the Coulomb friction model to simulate contact interactions during sliding. The mean values of force-displacement curves obtained experimentally under the normal loading condition (stationary finger) for the rotation angle of $\theta_0 = 0°$ were used to estimate the initial values of Mooney-Rivlin material constants. The simulated elliptical fingerpad contact

TABLE II The coefficients k_F (N/mm^{m_F}), k_A(mm^2/N^{m_A}) and the exponents m_F and m_A (unitless) of the power-law models.

Subject	Rotation Angle (degree)	k_F	m_F	R^2 (δ versus F_n)	k_A	m_A	R^2 (F_n versus A_{app})
S_1	0	0.0935	2.7300	0.99	116.3	0.1998	0.92
	15	0.1991	2.3530	0.99	106.1	0.2219	0.94
	30	0.3120	2.2750	0.99	76.82	0.2463	0.96
	45	0.5168	2.0714	0.99	56.63	0.2704	0.94
S_2	0	0.2535	2.3430	0.98	95.22	0.2158	0.93
	15	0.3280	2.2780	0.99	86.11	0.2312	0.94
	30	0.7120	1.8660	0.99	58.03	0.2637	0.96
	45	0.9504	1.7510	0.99	37.54	0.2859	0.90

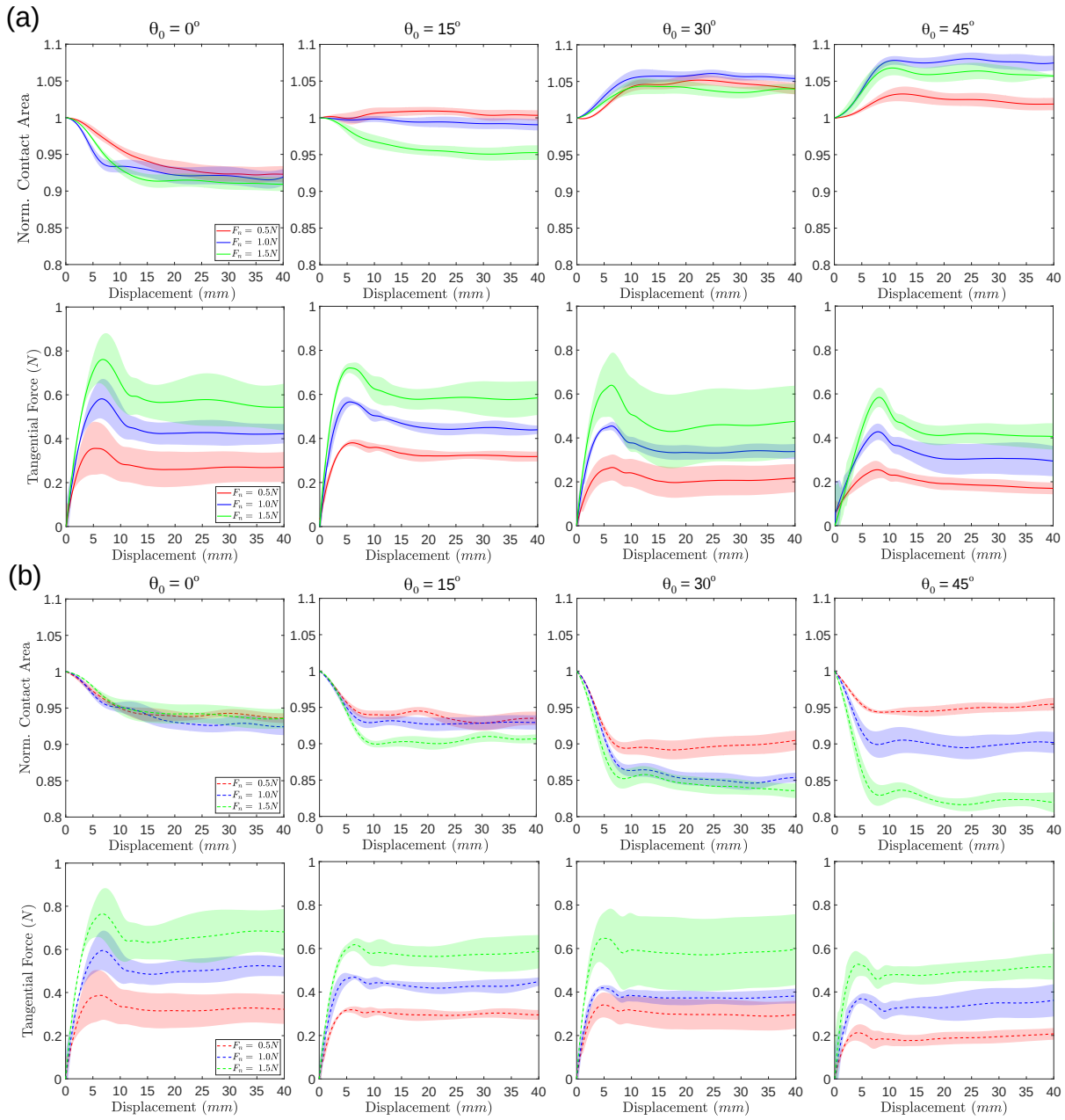

Fig. 6 Change in normalized apparent contact area and tangential force as a function of displacement during sliding in (a) ulnar direction, and (b) radial direction for rotation angles of 0°, 15°, 30°, and 45°. Solid and dashed lines are the mean values of the subjects, while the shaded regions around the mean values represent the standard deviations.

area, corresponding to the actual elliptical contact area illustrated in Fig. 4b, was calculated using the relation $A_{app} = \pi r_0 r_1$. In Fig. 4b, r_0 represents half of the simulated contact width (corresponding to w in Fig. 4b) between the SC and the plate, which varies with loading, and r_1 is half of the average fingerpad contact length ($l = 12.5$ mm), which was obtained from the fingerpad images of subject S_1 under the normal force of 1 N.

The FEM simulations were performed for 4 rotation angles of the finger under 2 conditions: i) normal loading (the plate was incrementally pushed upwards to compress the fingerpad), and ii) combined loading (the finger slid on the plate in ulnar and radial directions under a normal force of 1 N). The normal force as a function of vertical displacement (fingerpad compression) and apparent contact area as a function of normal force were recorded under the simulated normal loading condition (stationary finger). Apparent contact area and normal and tangential forces as a function of horizontal displacement were recorded under the simulated combined loading condition (sliding finger).

III. Results

A. Experimental results

In the first experiment (stationary finger under normal loading), the images of the fingerpad, the normal force acting on the finger, and the vertical displacement of the plate relative to the fingerpad were recorded in 3 separate sessions on 3 different days (4 rotation angles × 3 repetitions = 12 trials) for each subject. Fig. 5a and c illustrate the change in normal force as a function of the vertical displacement of the plate for S_1 and S_2, respectively. The normal force increases

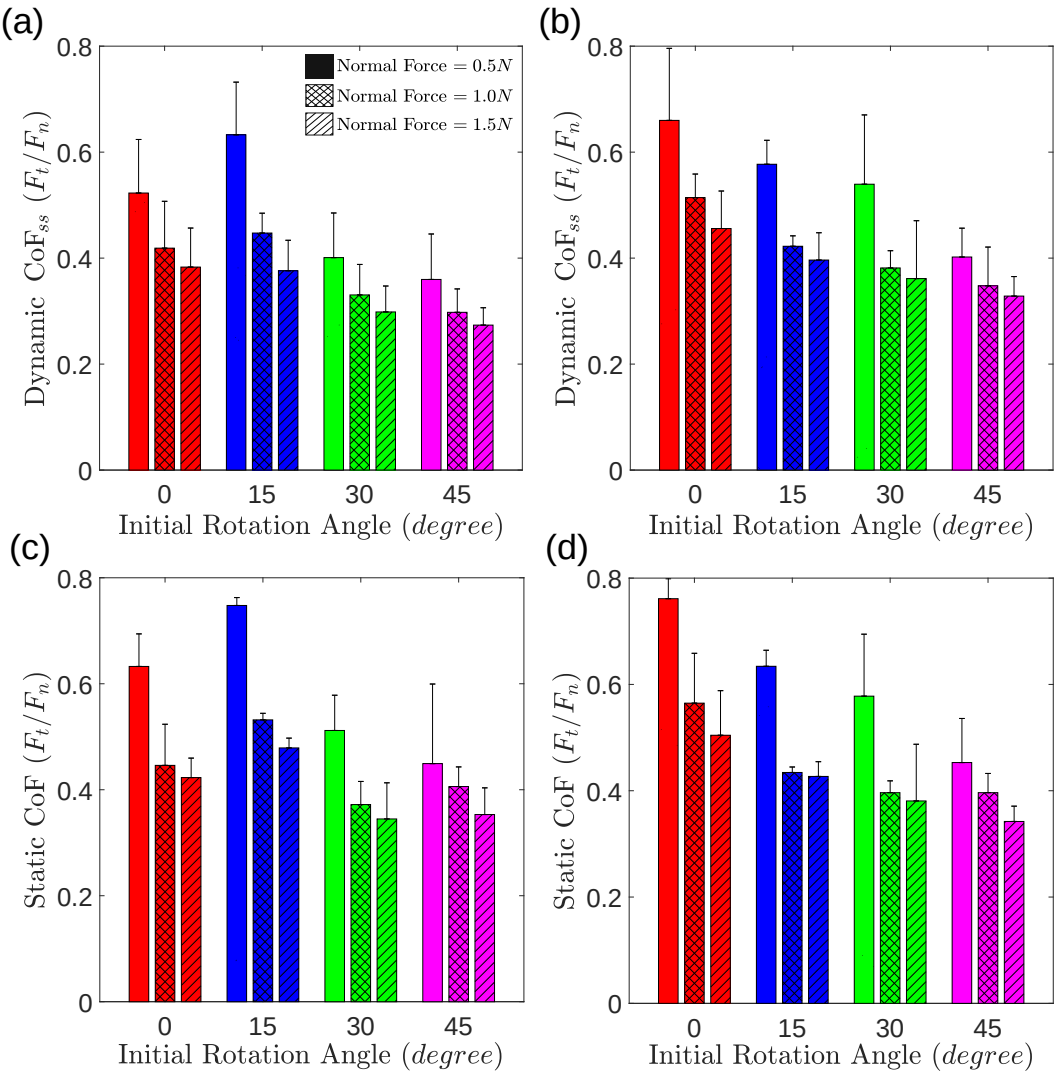

Fig. 7 Mean values of CoF with standard deviations for 4 different rotation angles and 3 different normal forces: dynamic CoF for ulnar and radial directions (a, b) and static CoF for ulnar and radial directions (c, d).

non-linearly with the displacement for all rotation angles (0°, 15°, 30°, and 45°). In addition, the magnitude of normal force increases as the rotation angle is increased. Fig. 5b and d depict the change in apparent contact area as a function of normal force for S_1 and S_2, respectively. The apparent contact area increases with normal force and nearly saturates at higher normal forces for all rotation angles. In addition, the size of the apparent contact area decreases as the rotation angle is increased.

A power-law model was fitted to the experimental data of displacement versus force and normal force versus apparent contact area:

$$F_n = k_F \delta^{(m_F)} \tag{1}$$

$$A^0_{app} = k_A {F_n}^{(m_A)} \tag{2}$$

where, m_i and k_i ($i = F, A$) are the exponents and coefficients of the model, respectively. A^0_{app} is the initial apparent contact area and δ is the vertical displacement for the stationary finger (no sliding). The results of the best-fitted curves are presented in Fig. 5 and the values of m_i and k_i are tabulated in Table II. For both subjects, increasing the rotation angle increases the displacement coefficient k_F and decreases the displacement exponent m_F, whereas it decreases the load coefficient k_A and increases the load exponent m_A. It is worth noting that the values of coefficients and exponents differ for S_1 and S_2, showing the subject-dependent effects due to the differences in material properties of finger and its morphology such as size and shape [1], [39]. For example, the minor and major radii of index finger cross-section for S_1 are 6.14 ± 0.02 mm and 8.55 ± 0.02 mm, and for S_2 are 5.95 ± 0.02 mm and 7.49 ± 0.02 mm, respectively.

For the combined loading condition (sliding finger), the images of the fingerpad and normal and tangential forces acting on the fingerpad were acquired in 72 trials from each participant, involving 4 rotation angles, 3 normal forces, 2 sliding directions, and 3 repetitions (the experiments were performed in 3 separate sessions on 3 different days). Fig. 6a and b present the normalized mean values of the apparent contact area (A_{app}/A^0_{app}) and the mean values of tangential forces for the ulnar and radial sliding directions, respectively. For the sliding in the radial direction, the apparent contact area decreases for all rotation angles. This reduction begins at the onset of the application of tangential force and persists until the macroscopic sliding regime is attained, at which point A_{app} stabilizes around its minimum value. For the rotation angles of 30° and 45°, A_{app} increases for sliding in the ulnar direction under all 3 normal forces. During the ulnar sliding at 15° rotation angle, A_{app} remains almost constant under the normal forces of 0.5 N and 1 N, but a slight

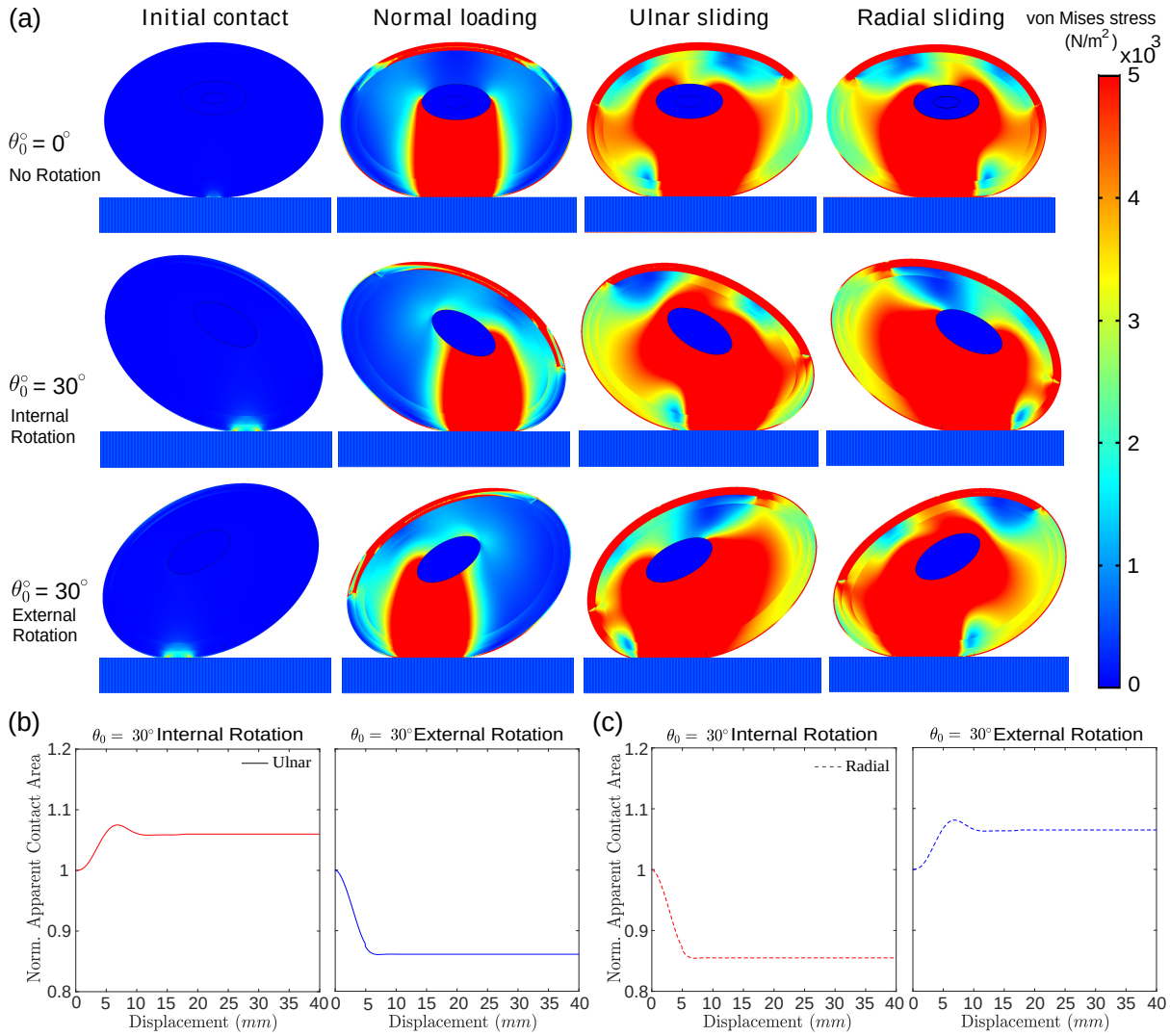

Fig. 8 (a) FEM simulations of the fingerpad under normal and combined loading conditions for the rotation angles of 0° (first row), 30° internal rotation (second row), and 30° external rotation (third row). A normal force of 1 N was applied and maintained for 30 seconds followed by horizontal sliding of the finger. The images present von Mises stress distribution across the fingerpad for initial contact, normal loading, and combined loading for sliding in ulnar and radial directions. Change in the apparent contact area as a function of displacement for 30° internal and external rotations during sliding in (b) ulnar and (c) radial directions. The mean values of CoF reported in Fig. 7 were used in the simulations for the contact interface.

reduction of approximately 3% is observed for a normal force of 1.5 N. On the other hand, the results show that regardless of the sliding direction, the static and dynamic (steady-state) CoF decreases as normal force and rotation angle increase (Fig. 7a-d). In addition, the mean values of steady-state CoF for radial sliding were consistently higher than those for ulnar sliding for all rotation angles and normal forces except for the rotation angle of 15°.

B. Finite element modeling results

Fig. 8 shows the FEM simulations of the fingerpad in contact with a flat plate under normal loading and combined loading conditions for 0° (first row), 30° internal rotation (second row), and 30° external rotation (third row) of the finger. To replicate the normal loading condition, the plate was moved in the vertical direction and incrementally compressed the stationary finger. In the sliding condition (combined loading), first, a normal force of 1 N was applied and maintained by regulating the vertical movement of the plate against the stationary finger for 30 seconds. Subsequently, the plate was slid in the ulnar/radial direction, inducing tangential traction on the fingerpad as a result of friction between the fingerpad and the plate. The mean CoFs obtained experimentally at different rotation angles (Fig. 7a-d) were utilized in the corresponding simulations. The images in Fig. 8a show von Mises stress distribution across the cross-section of the finger for initial contact, normal loading, and combined loading during sliding in ulnar and radial directions. Fig. 8b and c illustrate the change in apparent contact area as a function of displacement for 30° internal and external rotations during sliding in the ulnar and radial directions, respectively. Notably, for both ulnar and radial directions, the change in the apparent contact area during internal rotation exhibits an opposite trend to that observed during external rotation of the finger.

The change in normal force as a function of vertical displacement (compression of the fingerpad by the plate) and the change in apparent contact area as a function of normal force for 4 rotation angles are presented in Fig. 9a and b, respectively. The trends observed in FEM simulations match well with those of the experimental results reported in Fig. 5.

The simulation results for the apparent contact area under the

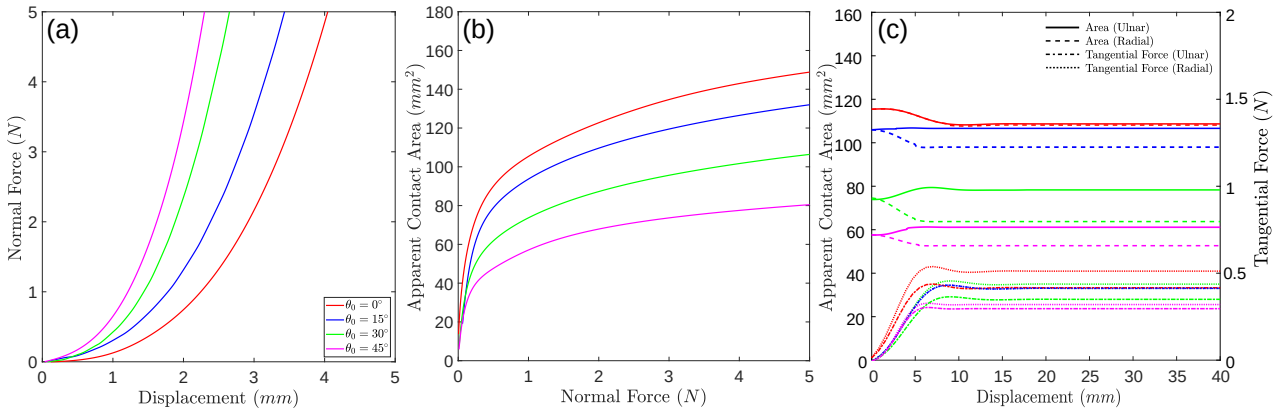

Fig. 9 Results of the FEM simulations: (a) change in normal force as a function of plate displacement and (b) change in apparent contact area as a function of normal force under normal loading condition (stationary finger). (c) Change in apparent contact area as a function of displacement for 4 rotations of the finger under combined loading condition (sliding finger).

sliding condition are presented in Fig. 9c, which are in line with the experimental results reported in Fig. 6. For the rotation angle of 0°, the apparent contact area, A_{app}, shrinks and eventually reaches a steady-state value during sliding in ulnar and radial directions. However, A_{app} increases during the ulnar sliding while it still decreases during the radial sliding for the rotation angles of 30° and 45°, as observed in the experiments. For the rotation angle of 15°, A_{app} remains almost constant during the ulnar sliding and decreases during the radial sliding with trends similar to the corresponding experimental results.

IV. Discussion

The main focus of this study was to examine how the initial rotation of the finger around the distal axis affects the evolution of the apparent contact area. The experimental investigation was carried out under two conditions: normal loading with a stationary finger, and combined normal and tangential loading while the plate was slid beneath the fingerpad in the ulnar and radial directions.

The change in normal force as a function of displacement under normal loading was modeled by a power-law function (Eq. 1), but the displacement exponents (m_F) estimated from the experimental data for 4 rotation angles are different from the Hertzian displacement exponent of 3/2, as also observed in the earlier studies [40]. Similarly, the load exponents (m_A) estimated from the experimental data of normal force versus apparent contact area for 4 rotation angles also differ from the Hertzian load exponent of 2/3 [41]. We observed that, under normal loading, the apparent contact area is reduced and the finger becomes stiffer as the rotation angle is increased (Fig. 5). This suggests that there are greater geometric constraints closer to the radial edge compared to the palmar edge. Even though the experimental data shows that the contact behavior is non-Hertzian, this stiffening behavior can be better visualized if the effective elastic modulus, E^*, is calculated based on the Hertz model using the following equation:

$$E^* = \frac{3F_n}{4\delta}\left[\frac{\pi}{A^0_{app}}\right]^{1/2} \tag{3}$$

Eq. 3 was utilized to calculate the effective elastic modulus of the fingerpad as a function of normal force using the experimental

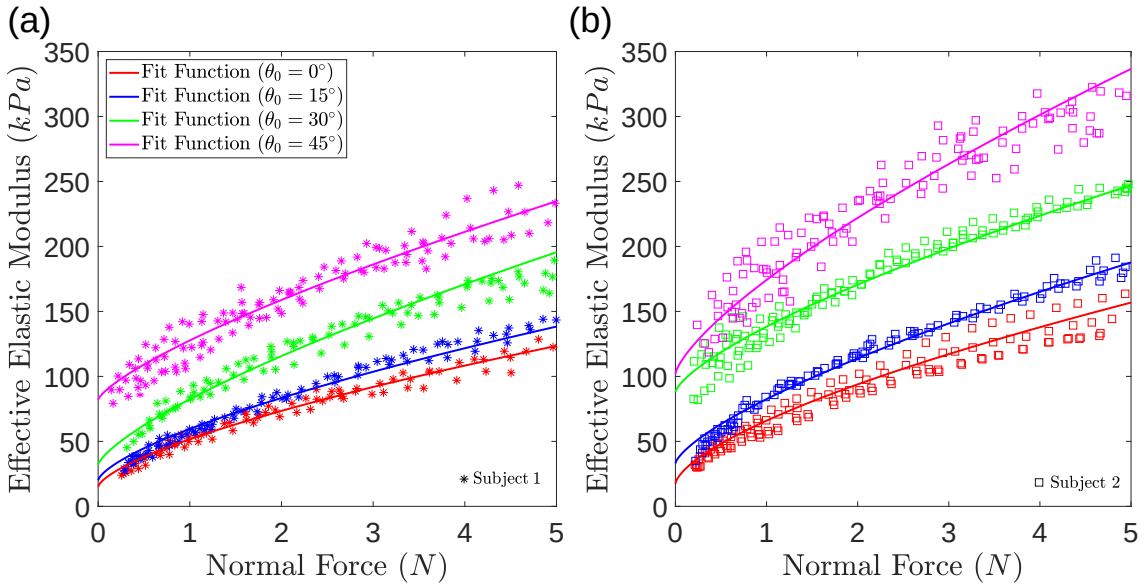

Fig. 10 Effective elastic modulus of the fingerpad as a function of normal force based on the experimental data collected under normal loading condition (a) for S_1, and (b) for S_2.

TABLE III Initial elastic modulus, E_0 (kPa), coefficient of normal force β (kN$^{(1-\gamma)}$/m^2), and normal force exponent γ (unitless) shown in Fig. 10.

Subject	Rotation Angle (degree)	E_0	β	γ	R^2
S_1	0	15	36.64	0.674	0.94
	15	20	39.55	0.681	0.96
	30	32	50.36	0.732	0.91
	45	82	45.64	0.751	0.93
S_2	0	25	41.26	0.635	0.98
	15	33	52.74	0.657	0.96
	30	88	53.21	0.676	0.83
	45	102	87.75	0.732	0.84

data collected for the normal loading condition. Table III tabulates the coefficients (E_0 and β) and exponent (γ) estimated from the experimental data by fitting a power-law model of $E^* = E_0 + \beta F_n^{\gamma}$. The results presented in Fig. 10 show an increase in the effective elastic modulus of the fingerpad as a function of normal force, while the increase in elastic modulus as a function of rotation angle appears to be non-linear. Dzidek et al. [17] reported a linear relation between the secant modulus and normal force for the contacts between the fingerpad and a smooth surface. They argued that the secant modulus approaches Young's modulus as F_n approaches zero. Moreover, across all experimental conditions, the effective elastic modulus values of S_1 are consistently lower than that of S_2. This discrepancy is attributed to larger apparent contact areas for S_1 compared to S_2 in addition to some other influencing factors [1], [42]. Our results show that the effective elastic modulus of the fingerpad changes with finger rotation about its axial axis, which impels us to consider its effect in developing analytical models interpreting the evolution of apparent contact area as a function of normal force.

The latter part of this study focused on the anisotropic change in the apparent contact area of the fingerpad during sliding in ulnar and radial directions for 4 different axial rotations of the finger. For the rotation angle of 0°, reduction in A_{app} starts at the onset of sliding in both ulnar and radial directions. The reduction in the apparent area as a function of displacement observed in our experiments for 0° rotation angle (Fig. 6a) is similar to those observed in the earlier experimental studies [29]–[31]. The reduction in apparent area is roughly equal to each other for the ulnar (7.8%) and radial (7.3%) sliding directions in our experiments. This similarity can be attributed to the symmetry in finger geometry and contact loading at 0° rotation angle. Sahli et al. [30] proposed an empirical relation for the reduction in area as a function of tangential force observed during sliding of a soft sphere on a rigid plate, in which the contact region evolves from a circular area under pure normal load to a reduced elliptical area in the macroscopic sliding regime. However, this relation loses its applicability to sliding contact between an initially rotated finger and a plate because of the changes in the radius of curvature and the asymmetries in contact loading, as observed in our study.

Non-linear stiffening of the fingerpad's skin and its finite deformations, which induce strong coupling between normal and tangential effects, have been reported among the causes behind the shear-induced area reduction [29], [32], [43]. In particular, contact lifting at the trailing edge was reported to contribute 90-95% to the total area reduction in [32]. Through FEM simulations of the sliding finger under electroadhesion, Forsbach et al. [44] reported a reduction of 12% in contact length. They showed that the increased tangential loading due to electroadhesion results in a torsional motion of the

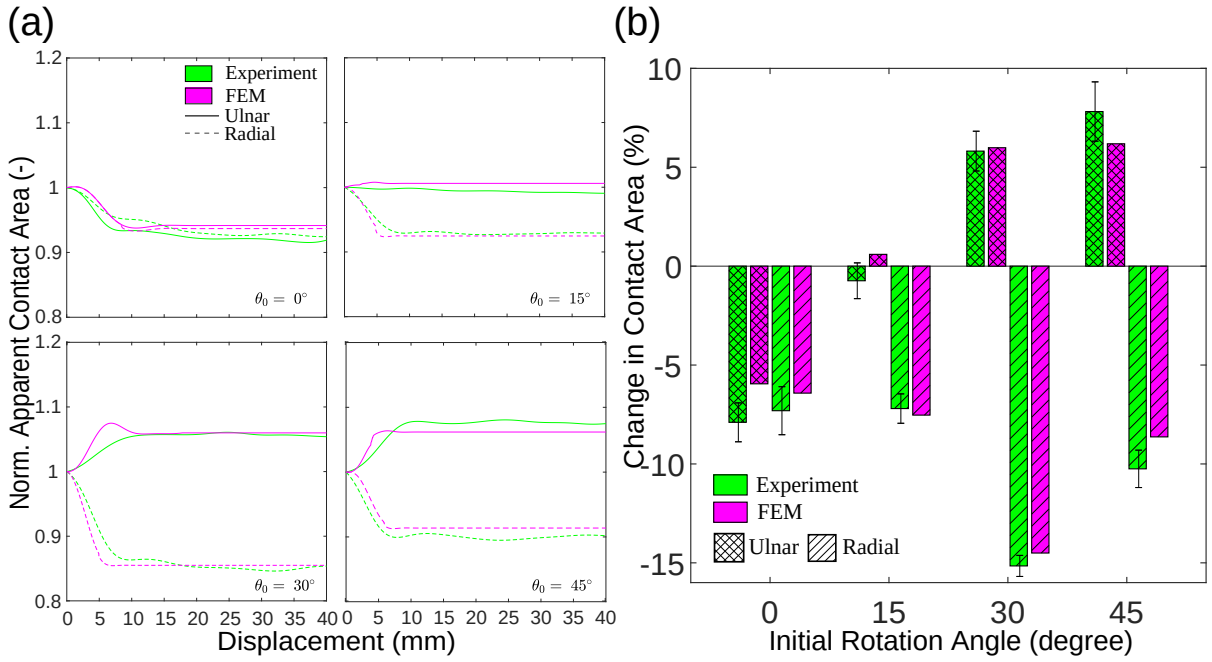

Fig. 11 Comparison between experimental and FEM results. The curves depicting the experimental data are derived from the average of two subjects. (a) Normalized apparent contact area as a function of displacement for ulnar and radial directions and (b) percentage change in contact area, with corresponding standard deviations for experimental results, as a function of the rotation angles for sliding in ulnar and radial directions.

tissue around the underlying bone of the fingertip, causing the ridges at the trailing edge to lift while new ridges contact the surface at the leading edge. The contact area changes reported in [44] are similar to those in the combined loading condition in our study. However, our FEM model did not include finger ridges, preventing the observation of staircase-like variations in contact area. Similarly, du Bois de Dunilac et al. [45] reported a $15 \pm 11\%$ reduction in the apparent contact area of the fingerpad under torsional loading about the palmar axis. They argued that the reduction was mainly driven by two mechanisms: peeling, where the fingerpad skin loses contact with the plate, and deformation due to in-plane skin compression, measured by computer vision techniques. Peeling was identified as the dominant factor contributing to the area change in their study.

In our study, the amount of reduction in contact area was influenced by the rotation angle during radial sliding and the relation between them was not linear. Our experimental results for the radial direction were supported by the FEM simulations (see the comparisons in Fig. 11a). A reduction of 7.3%, 7.2%, 15.1%, and 10.2% was observed in apparent area at 0°, 15°, 30°, and 45° rotation angles, respectively (Fig. 11b). On the other hand, during ulnar sliding, the change in contact area progressively shifted from a decrease at 0° (7.8% reduction) to a negligible change (0.7% reduction) at 15°, followed by an increase of 5.8% and 7.8% at the rotation angles of 30° and 45°, respectively (Fig. 11b). The experimental results on the ulnar direction are also supported by the FEM simulations (Fig. 11b). The increase in the apparent contact area for the rotation angles of 30° and 45° is surprising and has not been reported in the literature before. As suggested in [29], [32], the stiffening of the fingerpad appears to play a role in area change since Fig. 10 shows that the effective elastic modulus of the fingerpad increases non-linearly as the rotation angle is increased. The stiffening and relaxation of the fingerpad skin in varying degrees in response to the respective increase and decrease in the tangential forces cause a change in the apparent contact area and non-uniform stress distribution at the contact as analyzed by computer vision techniques in [33], [46].

We argue that the initial finger rotation around its distal axis introduces contact asymmetries due to changes in the radius of curvature and effective elastic modulus. These asymmetries influence the contact area under both normal and combined loading conditions. With an initial rotation of 30° and 45°, the index finger rotates further toward the middle finger during the onset of ulnar sliding, thereby increasing the radius of curvature and consequently increasing the apparent contact area. Additionally, variations in effective elastic modulus from radial to palmar edge create asymmetric stress distribution at the fingerpad's leading and trailing edges, as shown in our FEM simulations (see Fig. 8), contributing to anisotropic changes in the contact area. These findings highlight the importance of accounting for changes in the finger's contact area due to rotation when designing tactile displays and robotic hands to mimic human hand physiology better.

We also observed that the dynamic (steady-state) CoF decreases as the normal load is increased (see Fig. 7), showing the stronger effect of adhesion at low normal forces as reported in [2], [25]. On the other hand, the stiffening of the finger with an increase in rotation angle also results in a decrease in the steady-state CoF, possibly due to a large drop in the apparent contact area at higher rotation angles.

V. Conclusion

Investigating the contact mechanics between the human fingerpad and a smooth surface during sliding is an open area of research. In this paper, we performed experiments to investigate the rotation-dependent evolution of the contact area between the index finger and a smooth flat surface under normal loading (stationary finger) and combined loading (sliding finger) conditions. The experimental results were validated by FEM simulations. The experimental and FEM results support each other and show a reduction in the apparent contact area for the radial sliding direction while a surprising increase for the ulnar direction at higher rotation angles. This result suggests that the changes in contact geometry (due to the changes in the equivalent radius of curvature with the rotation of the finger) and material properties (due to the stiffening of the fingerpad as the rotation angle increases) cause an asymmetric change in contact area for the radial and ulnar directions. The findings of this study help improve our understanding of how we touch, explore, and manipulate objects around us in our daily lives.

In our current study, the change in the equivalent radius of curvature and material properties due to the rotation of the finger were coupled due to its morphological structure. In the future, we plan to mold spherical and ellipsoidal elastomer samples with varying material properties to investigate their distinct contribution to the anisotropic change in contact area, which we believe, will further improve our understanding of the contact mechanics between human fingerpad and a smooth flat surface.

Appendix A Supplementary Data

All the data and scripts used in this study are accessible through the Zenodo repository: https://doi.org/10.5281/zenodo.8195546.

Acknowledgment

C.B. acknowledges the financial support provided by TUBITAK under contract no. 117E954 for the development of the experimental setup used in this study.

References

[1] S. Derler and L.-C. Gerhardt, "Tribology of skin: Review and analysis of experimental results for the friction coefficient of human skin," *Tribology Letters*, vol. 45, no. 1, pp. 1–27, 2012.

[2] C. Basdogan, M. R. A. Sormoli, and O. Sirin, "Modeling sliding friction between human finger and touchscreen under electroadhesion," *IEEE Transactions on Haptics*, vol. 13, no. 3, pp. 511–521, 2020.

[3] V. Babin and C. Gosselin, "Mechanisms for robotic grasping and manipulation," *Annual Review of Control, Robotics, and Autonomous Systems*, vol. 4, pp. 573–593, 2021.

[4] K. L. Johnson, K. Kendall, and a. Roberts, "Surface energy and the contact of elastic solids," *Proceedings of the Royal Society of London. A. Mathematical and Physical Sciences*, vol. 324, no. 1558, pp. 301–313, 1971.

[5] B. V. Derjaguin, V. M. Muller, and Y. P. Toporov, "Effect of contact deformations on the adhesion of particles," *Journal of Colloid and Interface Science*, vol. 53, no. 2, pp. 314–326, 1975.

[6] D. Tabor, "Surface forces and surface interactions," in *Plenary and Invited Lectures*, Elsevier, 1977, pp. 3–14.

[7] J. A. Greenwood and J. P. Williamson, "Contact of nominally flat surfaces," *Proceedings of the Royal Society of London. Series A. Mathematical and Physical Sciences*, vol. 295, no. 1442, pp. 300–319, 1966.

[8] B. N. Persson, "Theory of rubber friction and contact mechanics," *The Journal of Chemical Physics*, vol. 115, no. 8, pp. 3840–3861, 2001.

[9] B. Persson, A. Kovalev, and S. Gorb, "Contact mechanics and friction on dry and wet human skin," *Tribology Letters*, vol. 50, no. 1, pp. 17–30, 2013.

[10] M. J. Adams, B. J. Briscoe, and S. A. Johnson, "Friction and lubrication of human skin," *Tribology Letters*, vol. 26, no. 3, pp. 239–253, 2007.

[11] E. AliAbbasi, M. Muzammil, O. Sirin, P. Lefévre, Ø. G. Martinsen, and C. Basdogan, "Effect of finger moisture on tactile perception of electroadhesion," *IEEE Transactions on Haptics*, 2024. DOI: 10.1109/TOH.2024.3441670.

[12] G. Serhat, Y. Vardar, and K. J. Kuchenbecker, "Contact evolution of dry and hydrated fingertips at initial touch," *PLoS ONE*, vol. 17, no. 7, e0269722, 2022.

[13] H. Gray, *Anatomy of the human body*. Lea & Febiger, 1878, vol. 8.

[14] D. Fawcett, "Hypophysis," *A textbook of histology, 11th Ed. Philadelphia, WB Saunders Co*, pp. 479–499, 1986.

[15] W. A. WA, "Biaxial tension test of human skin in vivo.," *Bio-Medical Materials and Engineering*, vol. 4, no. 7, pp. 473–486, 1994.

[16] M. B. Rubin, S. R. Bodner, and N. S. Binur, "An elastic–viscoplastic model for excised facial tissues," *Journal of Biomechanical Engineering*, vol. 120, no. 5, pp. 686–689, Oct. 1998.

[17] B. M. Dzidek, M. J. Adams, J. W. Andrews, Z. Zhang, and S. A. Johnson, "Contact mechanics of the human finger pad under compressive loads," *Journal of The Royal Society Interface*, vol. 14, no. 127, p. 20 160 935, 2017.

[18] M. Nosonovsky and B. Bhushan, "Multiscale friction mechanisms and hierarchical surfaces in nano-and bio-tribology," *Materials Science and Engineering: R: Reports*, vol. 58, no. 3-5, pp. 162–193, 2007.

[19] S. M. Pasumarty, S. A. Johnson, S. A. Watson, and M. J. Adams, "Friction of the human finger pad: Influence of moisture, occlusion and velocity," *Tribology Letters*, vol. 44, pp. 117–137, 2011.

[20] M. J. Adams, S. A. Johnson, P. Lefèvre, *et al.*, "Finger pad friction and its role in grip and touch," *Journal of The Royal Society Interface*, vol. 10, no. 80, p. 20 120 467, 2013.

[21] J. C. Mergel, R. Sahli, J. Scheibert, and R. A. Sauer, "Continuum contact models for coupled adhesion and friction," *The Journal of Adhesion*, vol. 95, no. 12, pp. 1101–1133, 2019.

[22] R. Sahli, G. Pallares, A. Papangelo, *et al.*, "Shear-induced anisotropy in rough elastomer contact," *Physical Review Letters*, vol. 122, no. 21, p. 214 301, 2019.

[23] J. C. Mergel, J. Scheibert, and R. A. Sauer, "Contact with coupled adhesion and friction: Computational framework, applications, and new insights," *Journal of the Mechanics and Physics of Solids*, vol. 146, p. 104 194, 2021.

[24] E. AliAbbasi, V. Aydingul, A. Sezgin, U. Er, S. Turkuz, and C. Basdogan, "Tactile perception of coated smooth surfaces," *IEEE Transactions on Haptics*, vol. 16, no. 4, pp. 586–593, 2023.

[25] S. Derler, L.-C. Gerhardt, A. Lenz, E. Bertaux, and M. Hadad, "Friction of human skin against smooth and rough glass as a function of the contact pressure," *Tribology International*, vol. 42, no. 11-12, pp. 1565–1574, 2009.

[26] L. Skedung, K. Danerlöv, U. Olofsson, *et al.*, "Tactile perception: Finger friction, surface roughness and perceived coarseness," *Tribology International*, vol. 44, no. 5, pp. 505–512, 2011.

[27] S. Maegawa, F. Itoigawa, and T. Nakamura, "Effect of normal load on friction coefficient for sliding contact between rough rubber surface and rigid smooth plane," *Tribology International*, vol. 92, pp. 335–343, 2015.

[28] X. Zhou, J. L. Mo, Y. Y. Li, *et al.*, "Effect of finger sliding direction on tactile perception, friction and dynamics," *Tribology Letters*, vol. 68, pp. 1–13, 2020.

[29] B. Delhaye, P. Lefevre, and J.-L. Thonnard, "Dynamics of fingertip contact during the onset of tangential slip," *Journal of The Royal Society Interface*, vol. 11, no. 100, p. 20 140 698, 2014.

[30] R. Sahli, G. Pallares, C. Ducottet, *et al.*, "Evolution of real contact area under shear and the value of static friction of soft materials," *Proceedings of the National Academy of Sciences*, vol. 115, no. 3, pp. 471–476, 2018.

[31] O. Sirin, A. Barrea, P. Lefèvre, J.-L. Thonnard, and C. Basdogan, "Fingerpad contact evolution under electrovibration," *Journal of the Royal Society Interface*, vol. 16, no. 156, p. 20 190 166, 2019.

[32] J. Lengiewicz, M. de Souza, M. A. Lahmar, *et al.*, "Finite deformations govern the anisotropic shear-induced area reduction of soft elastic contacts," *Journal of the Mechanics and Physics of Solids*, vol. 143, p. 104 056, 2020.

[33] I. Ozdamar, M. R. Alipour, B. P. Delhaye, P. Lefevre, and C. Basdogan, "Step-change in friction under electrovibration," *IEEE Transactions on Haptics*, vol. 13, no. 1, pp. 137–143, 2020.

[34] E. AliAbbasi, M. A. Sormoli, and C. Basdogan, "Frequency-dependent behavior of electrostatic forces between human finger and touch screen under electroadhesion," *IEEE Transactions on Haptics*, vol. 15, no. 2, pp. 416–428, 2022.

[35] T. Maeno, K. Kobayashi, and N. Yamazaki, "Relationship between the structure of human finger tissue and the location of tactile receptors," *JSME International Journal Series C Mechanical Systems, Machine Elements and Manufacturing*, vol. 41, no. 1, pp. 94–100, 1998.

[36] H. Fruhstorfer, U. Abel, C.-D. Garthe, and A. Knüttel, "Thickness of the stratum corneum of the volar fingertips," *Clinical Anatomy: The Official Journal of the American Association of Clinical Anatomists and the British Association of Clinical Anatomists*, vol. 13, no. 6, pp. 429–433, 2000.

[37] T. Vodlak, Z. Vidrih, E. Vezzoli, B. Lemaire-Semail, and D. Peric, "Multi-physics modelling and experimental validation of electrovibration based haptic devices," *Biotribology*, vol. 8, pp. 12–25, 2016.

[38] J. Z. Wu, D. E. Welcome, and R. G. Dong, "Three-dimensional finite element simulations of the mechanical response of the fingertip to static and dynamic compressions," *Computer Methods in Biomechanics and Biomedical Engineering*, vol. 9, no. 1, pp. 55–63, 2006.

[39] P.-H. Cornuault, L. Carpentier, M.-A. Bueno, J.-M. Cote, and G. Monteil, "Influence of physico-chemical, mechanical and morphological fingerpad properties on the frictional distinction of sticky/slippery surfaces," *Journal of The Royal Society Interface*, vol. 12, no. 110, p. 20 150 495, 2015.

[40] S. Tomlinson, R. Lewis, X. Liu, C. Texier, and M. Carré, "Understanding the friction mechanisms between the human finger and flat contacting surfaces in moist conditions," *Tribology Letters*, vol. 41, pp. 283–294, 2011.

[41] N. Huloux, L. Willemet, and M. Wiertlewski, "How to measure the area of real contact of skin on glass," *IEEE Transactions on Haptics*, vol. 14, no. 2, pp. 235–241, 2021.

[42] J. Van Kuilenburg, M. A. Masen, and E. Van Der Heide, "Contact modelling of human skin: What value to use for the modulus of elasticity?" *Proceedings of the Institution of Mechanical Engineers, Part J: Journal of Engineering Tribology*, vol. 227, no. 4, pp. 349–361, 2013.

[43] D. Babu, M. Konyo, H. Nagano, and S. Tadokoro, "Introducing whole finger effects in surface haptics: An extended stick-slip model incorporating finger stiffness," *IEEE Transactions on Haptics*, vol. 11, no. 3, pp. 417–430, 2018.

[44] F. Forsbach, M. Heß, and A. Papangelo, "A two-scale fem-bam approach for fingerpad friction under electroadhesion," *Frontiers in Mechanical Engineering*, vol. 8, p. 1 074 393, 2023.

[45] S. du Bois de Dunilac, D. Córdova Bulens, P. Lefèvre, S. J. Redmond, and B. P. Delhaye, "Biomechanics of the finger pad in response to torsion," *Journal of the Royal Society Interface*, vol. 20, no. 201, p. 20 220 809, 2023.

[46] B. Delhaye, A. Barrea, B. B. Edin, P. Lefevre, and J.-L. Thonnard, "Surface strain measurements of fingertip skin under shearing," *Journal of The Royal Society Interface*, vol. 13, no. 115, p. 20 150 874, 2016.

Jahangier Ahmad is a M.Sc. student in Mechanical Engineering program of Koc University in Istanbul, Turkey. He received his B.Sc. degree in Mechatronics Engineering from University of Engineering and Technology Taxila Pakistan in 2009. His research interests include surface haptics, finite element modeling, simulation, and analysis of dynamic systems.

Easa AliAbbasi is a postdoctoral researcher at Max Planck Institute for Informatics, Saarbrucken, Germany. He received the Ph.D. degree in Computational Sciences and Engineering from Koc University, Istanbul, Turkey in 2023, and the M.Sc. degree in Mechatronics Engineering from University of Tabriz, Tabriz, Iran in 2017. His research interests include haptics, human-computer interaction, tactile displays, and mechatronics.

MReza Alipour Sormoli received his B.Sc. degree from University of Tabriz in 2014, M.Sc. degree from the Amirkabir University of Technology (Tehran Polytechnic) in 2017, and is currently working toward a Ph.D. degree in Mechanical Engineering. His research interests include robotics, mechatronics, control, and dynamics.

Cagatay Basdogan received the Ph.D. degree in mechanical engineering from Southern Methodist University. He is a faculty member in the mechanical engineering and computational sciences and engineering programs at the College of Engineering, Koc University, Istanbul. Before joining Koc University, he worked at NASA-JPL/Caltech, the Massachusetts Institute of Technology, and Northwestern University Research Park. His research interests include haptic interfaces, robotics, mechatronics, biomechanics, medical simulation, computer graphics, and multi-modal virtual environments. In addition to serving on editorial boards of several journals and program committees of conferences, he chaired the IEEE World Haptics Conference in 2011.